Journal of Materials Chemistry A

ROYAL SOCIETY OF CHEMISTRY

PAPER

View Article Online
View Journal | View Issue

Cite this: J. Mater. Chem. A, 2024, 12, 20088

Wood-derived flexible supercapacitors for anti-freezing green power sources†

Hongting Ma,[a] Qian Zhao,[a] Peihao Cheng,[a] Xiaodong Geng,[a] Huannuo Tao,[a] Zhouxiaolong Zhang,[a] Yue Jiang,[a] Junlin Ma,[a] Kai Yang,[a] Quanli Liu,[a] Hanwen Zhang,[a] Zhida Liang,[b] Jian Li,*[c] Tianlu Wang,*[ade] Mianqi Xue *[f] and Nan Zhu *[a]

Received 4th April 2024
Accepted 26th June 2024

DOI: 10.1039/d4ta02190h

rsc.li/materials-a

Highly porous wood-derived electronics have attracted tremendous attention for the fabrication of high-performance supercapacitors (SCs) owing to their environmental benignity, natural abundance, renewability, and biodegradability. However, it is challenging to overcome the intrinsic rigidity and sluggish electrochemical reaction kinetics of wood-based SCs at low temperatures. Herein, we demonstrate an anti-freezing flexible SC (AF-FSC) based on delignified wood electrodes with an organohydrogen electrolyte. The chemical delignification process removes hemicellulose and lignin from natural wood, resulting in a softwood skeleton electrode. When assembled with a solid hydrogel electrolyte, the AF-FSC exhibits high mechanical flexibility over 93% capacitance retention after 1000 bending/twisting cycles at −30 °C. Besides, high areal capacitance (285.2 mF cm^{-2}) at −30 °C is achieved, which is higher than most wood derivatives operating at room temperature. The unique properties of the anti-freezing flexible AF-FSC make it a green renewable power source for driving multi-functional electronic components in real-life scenarios.

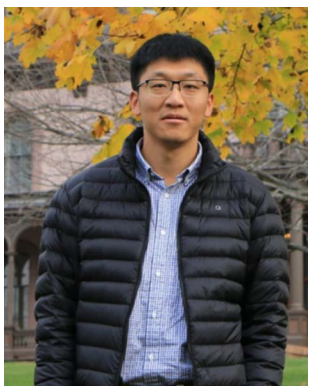

Nan Zhu

Nan Zhu, Professor, School of Chemistry, Dalian University of Technology (DUT), China. 2017 joined in DUT as an independent PI, and has established a research group of "Flexible wearable electrochemical biosensors and Nano energy device". Prof. Zhu previously worked as a Postdoc Researcher at University of California, San Diego, USA and University of Copenhagen, Denmark during 2013–2017; obtained PhD degree at Technical University of Denmark in 2013. Prof. Zhu's research interests are focused on wearable electrochemical biosensors (sweat/saliva/tear) and application in self-powered system.

1 Introduction

With the rapid growth of global energy demand, efficient energy storage devices, *e.g.*, supercapacitors (SCs),[1,2] lithium-ion batteries,[3,4] or lithium–air batteries,[5,6] have recently garnered enormous industrial and academic interests. Among these devices, SCs have moved to the center stage owing to their high power-density, excellent cycling stability, and fast charge–discharge properties.[7–9] To date, various favorable electrode materials, such as transition metal-based compounds,[10,11] metal hydroxides,[12,13] Prussian blue analogues[14,15] or large-sized carbonaceous materials,[16,17] have been studied and applied in high performance SCs. However, these inorganic compounds generally contain poisonous components that would lead to serious safety or environmental issues. Thus, exploring SC devices with green/sustainable strategies is critical for the development of advanced energy storage technology. Wood-derived micro-/nanomaterials, which are environmentally benign, naturally abundant, renewable, or biodegradable, have

[a]Cancer Hospital of Dalian University of Technology, School of Chemistry, Dalian University of Technology, 116024, Dalian, Liaoning, China. E-mail: nanzhu@dlut.edu.cn

[b]Department of Health Management, Dalian Rehabilitation Recuperation Center of Joint Logistics Support Force of PLA, 116013, Dalian, China

[c]Center for Reproductive Medicine, Dalian Women and Children's Medical Center (Group), 116037, Dalian, China. E-mail: dlfclj@126.com

[d]Department of Radiotherapy, Cancer Hospital of China Medical University, Liaoning, Cancer Hospital & Institute, Cancer Hospital of Dalian University of Technology, No. 44, Xiaoheyan Road, Dadong District, Shenyang, 110042, Liaoning Province, China. E-mail: wangtianlu@cancerhosp-ln-cmu.com

[e]Faculty of Medicine, Dalian University of Technology, Dalian 116024, China

[f]Technical Institute of Physics and Chemistry, Chinese Academy of Sciences, Beijing 100190, China. E-mail: xuemq@mail.ipc.ac.cn

† Electronic supplementary information (ESI) available: Details of experimental procedures and additional figures. See DOI: https://doi.org/10.1039/d4ta02190h

attracted significant interest.[18–20] Especially, straight channels in natural wood are suited for fast mass transport along channel directions, making wood derivatives suitable candidates for SCs.[21–23] Despite the tremendous progress being accomplished in the construction of high performance wood-based SCs, several challenges still limit their practical application, such as poor flexibility and low-temperature unavailability.

Consisting of cellulose nanofibers (CNFs) and amorphous matrix (lignin and hemicelluloses), natural woods are easily collapsed by the compact structure of a stiff cellulose skeleton.[24] As reported, lignin in wood could be removed to release tight connections between CNF bundles *via* chemical delignification, and delignified wood (DW) maintains its inherent structure of an aligned cellulose skeleton, realizing the high flexibility of wood-based electronics.[25,26] Impressive studies have been reported on the development of DW;[18,27,28] however, the development of flexible wood-derived high-performance SCs for wearable electronics is still in its infancy. Besides flexibility and good environmental adaptability, such as anti-freezing behavior, is also in urgent demand for SCs.[29,30] Dramatic decrease in energy storage capacity or flexibility in cold environments greatly limits the wide application of SCs.[31] Nevertheless, there are few studies on wood-based SCs under sub-zero temperatures, where the water content in conventional electrolytes is frozen. Therefore, developing an anti-freezing flexible SC (AF-FSC) based on sustainable wood derivatives is necessary.

Herein, the development of a green flexible wood SC with anti-freezing properties has been proposed. Through a simple chemical delignification process and alkali treatment, the stiff cellulose crystalline structure in natural wood is greatly swelled and softened, acquiring flexible wood skeletons, which are highly porous. Polypyrrole (PPy) is thus *in situ* grown both on the surface and inside channels of treated wood, resulting in high areal mass loading. Then, the anti-freezing property of AF-FSC was achieved by utilizing organohydrogel as a solid-state polyelectrolyte. Benefiting from the integrated structure with highly efficient electron/ion transport, AF-FSC achieves high areal capacitance at −30 °C (285.2 mF cm^{-2}), comparable with most wood-based SCs operating at room temperature. Furthermore, the intrinsic flexibility of both the wood-based electrode and polyelectrolyte contributes to the good mechanical performance of AF-FSC under 1000 bending/twisting cycles, even at low temperatures. Wood derivatives for fabrication of AF-FSC with high flexibility and anti-freezing behaviors pave a new way to develop green/sustainable energy storage devices for practical wearable electronics.

2 Experimental

2.1 Preparation of alkali-treated delignified wood (ADW)

ADW was prepared through two steps.[18] Firstly, natural balsa wood slices (20 × 20 × 1 mm^3) were immersed in a 2 wt% solution of sodium chlorite ($NaClO_2$) in acetic acid conditions (pH = 4.6) and heated to 80 °C for 6 h. After washing with distilled water several times, the delignified wood turned white. Secondly, ADW was achieved by delignifying the delignified wood (DW) slices in 15 wt% NaOH solutions at room temperature for 2 h and then washing with distilled water.

2.2 *In situ* growth of PPy on ADW

The PPy/ADW electrode was prepared through a chemical oxidative polymerization process. Briefly, the as-prepared ADW was immersed in 0.6 M pyrrole solution with dissolved (ammonium persulfate) APS (pyrrole/APS molar ratio = 1 : 2) at 4 °C for several hours. After complete polymerization of pyrrole, the electrode was taken out and washed with deionized water. The immersing time of ADW was 2, 4, 6, and 8 h for measuring the electrical performance of the PPy/ADW electrode.

2.3 Synthesis of AF-OHP

6 g of AM was dispersed in 20 mL of deionized water and then 0.003 g methylenebis-acrylamide was added to the solution. Secondly, 15 μL of *N*,*N*,*N*′,*N*′-tetramethyl-ethylenediamine (TMED) catalysts and 0.02 g of ammonium persulfate (APS) initiators were added to initiate the polymerization under stirring. The mixed solution was quickly poured into plastic vessels and reacted at 50 °C for 24 h to obtain cross-linked PAM hydrogel. To receive the AF-OHP hydrogel, PAM was dried at 60 °C for 6 h and then soaked in 10 wt% of sulfuric acid ethylene glycol/water (v/v = 1 : 1) solution for 24 h to achieve the equilibrated state.[29] PAM hydrogel polyelectrolyte was prepared by soaking the PAM hydrogel in 10 wt% of sulfuric acid aqueous solution for 24 h.

2.4 Fabrication of AF-FSC

Firstly, the AF-OHP electrolyte (12 × 12 × 1 mm^3) was put between two pieces of free-standing PPy/ADW electrode layers (12 × 10 × 1 mm^3). Secondly, two identical carbon cloth strips were tightly affixed to both sides of PPy/ADW as collectors. Similarly, different contrasted SCs (natural balsa wood-based SC or PAM-based SC) were fabricated using the same method.

2.5 Characterization

The morphology of natural balsa wood and ADW were observed by field emission scanning electron microscopy (FE-SEM, Carl Zeiss Ultra Plus, Germany) at an acceleration voltage of 5 kV. X-ray diffraction measurement (XRD, Rigaku D/MAX-2400 diffractometer), FTIR spectroscopy (Bruker VERTEX 700 spectrometer), Raman (Invia Qontor), and Mercury Penetration tests (AutoPore Iv 9510) were carried out to study the cellulose skeleton, and chemical composition changes of ADW and verify the existence of PPy in PPy/ADW.

2.6 Electrochemical measurements

The electrochemical performance of SCs was studied using an electrochemical workstation (CHI660E). The conductivity of PPy/ADW under bending/twisting or stretching processes was tested by *I*–*V* curves. The resistances were verified by the slope of the *I*–*V* curves.

To obtain the ionic conductivity, the AF-OHP hydrogel electrolyte was sandwiched between two stainless steel sheets. The

ionic conductivity σ (mS cm^{-1}) was calculated according to eqn (1):

$$\sigma = \frac{L}{R \cdot A} \times 1000 \quad (1)$$

σ is the ionic conductivity of the hydrogel electrolyte, and R, A and L are the bulk resistance, effective test area (1 cm^2) and thickness of the hydrogel electrolyte (0.1 cm), respectively.

GCD profiles, CV curves, and electrochemical impedance spectroscopy (EIS) measurements of SCs were carried out to study the capacitance performance of SCs. CV was tested at different scan rates of 50, 100, 150, 200 and 250 mV s^{-1}. GCD was measured at 2, 4, 6, 8, and 10 mA cm^{-2} current density. Specific areal capacitance (C_A) was calculated by eqn (2) from GCD curves:

$$C_A = \frac{I\Delta t}{S(V - IR_{drop})} \quad (2)$$

Here, S is the area (1 cm^2) of the device, V (V) is the potential window, I (A) is the applied discharge current, and Δt (s) is discharge time.

Energy density (E/W h cm^{-2}) and power density (P/W cm^{-2}) with respect to area were measured using eqn (3) and (4), respectively:

$$E = \frac{C_A(V - IR_{drop})^2}{2 \times 3600} \quad (3)$$

$$P = \frac{3600E}{\Delta t} \quad (4)$$

2.7 Electrolyte absorption ability (A) of PPy/ADW and PPy/mature wood

The totally dried samples were weighed (m_0) and then immersed in the electrolyte (before chemically cross-linked into PAM) for 5 min to reach saturated absorption under 20 °C (or −30 °C) and finally weighed instantaneously (m). Then, A can be determined by eqn (5):

$$A = \frac{m - m_0}{m_0} \quad (5)$$

3 Results and discussion

3.1 Characterization of wood-derived electrode and anti-freezing electrolyte

Fig. 1 illustrates the preparation of AF-FSC, with PPy-coated alkali-treated delignified wood (PPy/ADW) as electrodes and stretchable anti-freezing organohydrogel as polyelectrolyte (AF-OHP).

Natural balsa wood, consisting of a three-dimensional hierarchical skeleton with stiff lignin and hemicelluloses, is easily collapsed.[18,24] To increase flexibility, two chemical treatments were applied. Firstly, the delignification process was used to remove the lignin, releasing tight connections between CNF bundles while maintaining inherent structure.[20] The remaining lignin and hemicellulose were then degraded by alkali treatment.[32] Compared with natural balsa wood, which is easily

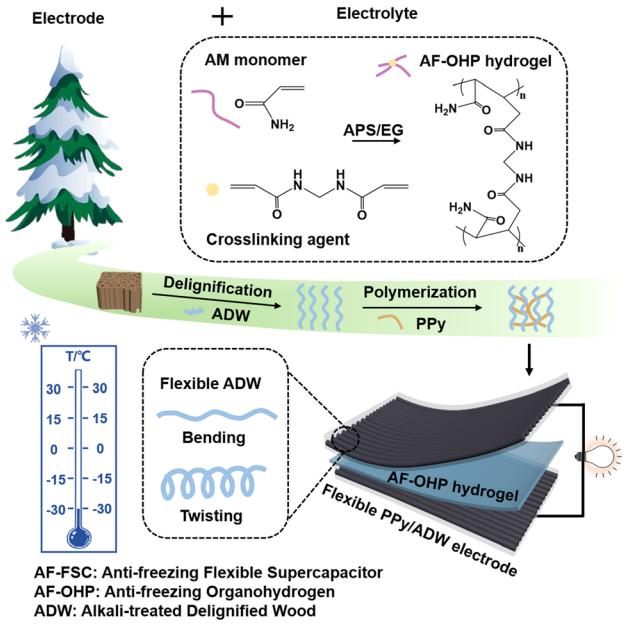

Fig. 1 Illustration of fabricating an anti-freezing flexible supercapacitor (AF-FSC) (AM: acrylamide; EG: ethylene glycol; AF-OHP: anti-freezing organohydrogen; ADW: alkali-treated delignified wood).

damaged, the as-obtained ADW showed extreme flexibility and could be folded along the growth direction without fracturing (Fig. 2a and b). Meanwhile, a highly porous structure was observed in cross-sections of ADW in SEM images due to wood matrix removal (Fig. 2c). Although native honeycomb-like cell structure was apparent for wood samples (Fig. S1†), ADW showed richer and bigger nano/microscale pores. Furthermore, PPy was utilized as an active material for AF-FSC due to its high conductivity and thermal stability.[33] As shown in Fig. 2d, PPy was *in situ* grown on both the surface and inside channels of ADW. The pore size distribution calculated using Mercury Penetration tests is given in Fig. 2e and f. Natural balsa wood possessed a specific surface area of 4.054 m^2 g^{-1} and a pore volume of 4.67 cm^3 g^{-1}, while PPy/ADW had a higher specific surface area of 32.69 m^2 g^{-1} and a pore volume of 4.83 cm^3 g^{-1}, respectively. Both balsa wood and PPy/ADW showed a high porosity of 83%, but the pore widths of PPy/ADW were obviously larger. An overwhelming number of the pore widths were centred at *ca.* 44 694 nm in the PPy/ADW electrode. Meanwhile, the pore size distributions of natural balsa wood were mainly at 663 nm. Increasing pore size indicates the successful removal of lignin and hemicelluloses in the wood's cell walls after alkali treatment. The high porous structural advantage of ADW loaded with more active materials per unit area benefits the construction of the PPy/ADW electrode with high conductivity. The conductivity of the PPy/ADW electrode was evaluated by IV curves (Fig. S2a†). The resistance decreased with increasing immersion time within 6 h, resulting from the gradual oxidation of pyrone. However, conductivity became stable upon 8 h immersion, attributed to the completely oxidized pyrone. Since the further extension of immersion time for excessive accumulation of PPy would lower the cyclic stability of AF-FSC,[34] 6 h was chosen as the optimal immersion time for the fabrication of

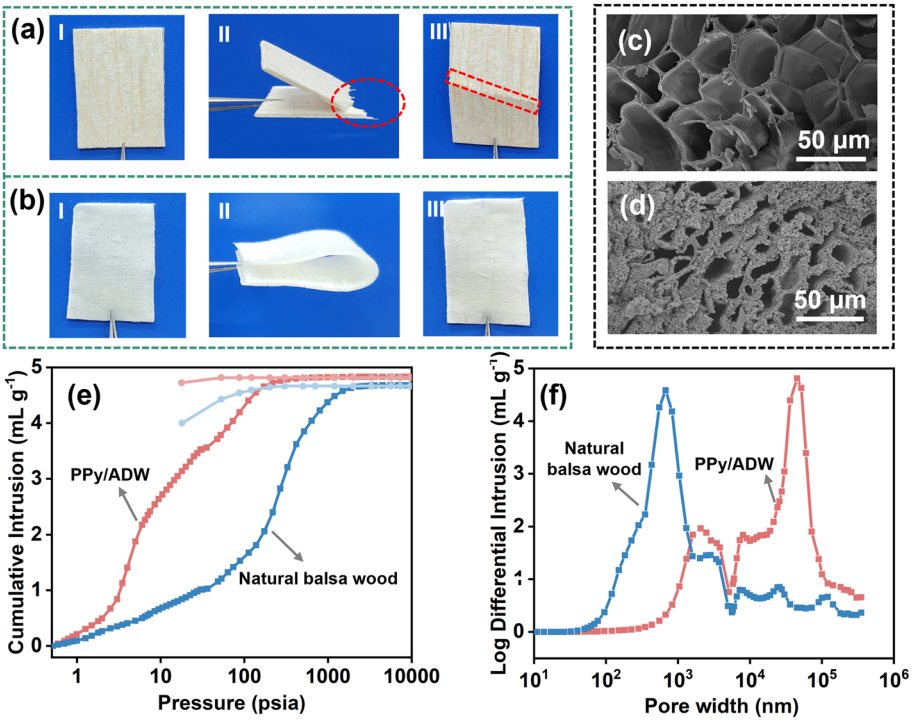

Fig. 2 Characterization of PPy/ADW and AF-OHP. Photographs of (a) a natural balsa wood slice and (b) ADW before (I), under (II), and after (III) bending. SEM images of (c) ADW and (d) PPy/ADW. (e) Mercury intrusion–extrusion cures and (f) pore size distributions of natural balsa wood and PPy/ADW electrode.

the PPy/AWD electrode. The conductivity remained stable during bending or twisting until 180° (Fig. S2b†), and there sometimes appeared negligible fluctuation because of the rising distance between PPy-coated CNFs. Meanwhile, PPy/ADW exhibited good flexibility, which showed no obvious fracture under 12% strain (Fig. S3a†). In comparison, natural balsa wood was bent to break under 12% strain (Fig. S3b†). More detailed characterization performance, such as Raman, XRD, and FTIR spectra of natural balsa wood, ADW and PPy/ADW are shown in Fig. S4.† Overall, excellent flexibility and electrical performance confirmed PPy/AWD as a suitable candidate to fabricate AF-FSC.

Then, the anti-freezing property of AF-FSC was achieved by employing AF-OHP as an electrolyte. Water in the hydrogel electrolyte was displaced by ethylene glycol (EG), leading to a decrease in saturated vapor pressure since EG could combine water molecules into stable organic molecular clusters.[35] The as-prepared AF-OHP showed outstanding flexibility with a mechanical strength of 16 kPa (Fig. S5a†), and it could be stretched to 300% even with temperature dropping to −30 °C (Fig. S5b and c†). Meanwhile, AF-OHP showed good intrinsic tackiness of organohydrogen polyelectrolyte, easily adhering to various substrates, such as glass and PPy/AWD electrode (Fig. S6†). Thus, adhesive strength enables direct attachment between the AF-OHP electrolyte and PPy/AWD electrodes avoiding extra binder.

3.2 Electrochemical performance of AF-FSC

Outstanding electronic and flexible performance of PPy/ADW and AF-OHP made them suitable candidates to fabricate AF-FSC. An ultralight solid-state AF-FSC was constructed *via* the assembly of PPy/ADW as electrodes and AF-OHP as the electrolyte, shown as standing on leaves (Fig. 3a). Owing to good flexibility of both the electrode and electrolyte, the as-prepared AF-FSC was highly flexible along the wood growth direction of ADW, and there was no crack observed after bending or twisting of AF-FSC (Fig. 3b and c). Furthermore, cyclic voltammetry (CV) and galvanostatic charge–discharge (GCD) were used to evaluate the electrochemical behaviors of AF-FSC at room temperature. Rectangular CV curves confirmed the fast charging/discharging property of AF-FSC with high power density (Fig. 3d).[36] Meanwhile, symmetrical shapes of GCD curves at different current densities (Fig. 3e) indicated high reversibility during the charging/discharging processes.[33] AF-FSC possessed a specific areal capacitance of 1034.94, 679.43, 504.94, 404.49 and 338.29 mF cm^{-2} at 2, 4, 6, 8 and 10 mA cm^{-2}, respectively (Fig. 3e). Compared with natural wood-based SC (Fig. S7†) and PET-based SC (0.152 mF cm^{-2} at 0.2 mA cm^{-2}, Fig S8†), higher capacitance of AF-FSC (504.94 mF cm^{-2}) demonstrated the effectively improved loading amount of *in situ* grown PPy. Specific energy density (E) and power density (P) of AF-FSC were also calculated from GCD curves (Fig. 3e) using eqn (3) and (4), exhibiting a large energy density of 66.13 μW h cm^{-2} at a power density of 708.39 μW cm^{-2} (Fig. S9†). Additionally, the energy density maintained a high value of 8.99 μW h cm^{-2} when the power density increased to 2186.7 μW cm^{-2}. The volume-specific capacitance, energy density, and power density are also listed in Table S1.†

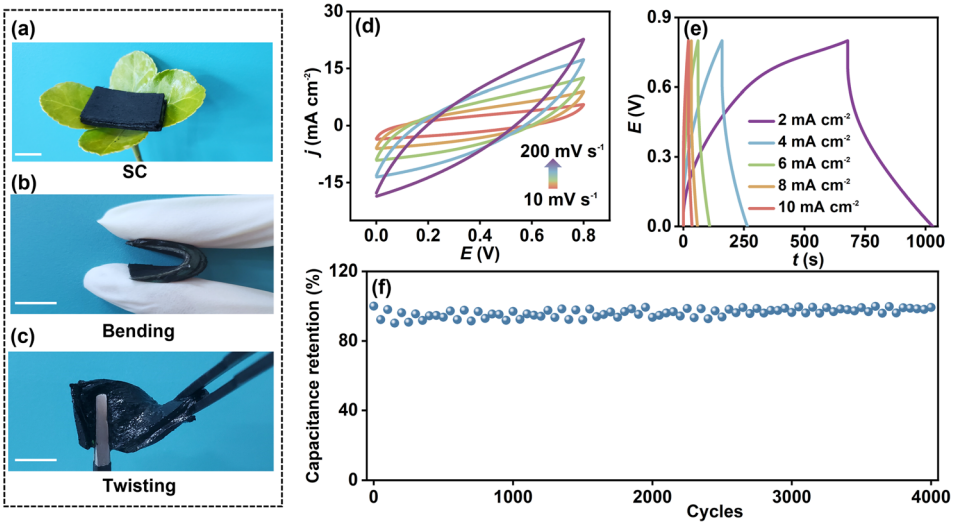

Fig. 3 Electrochemical performance of the prepared AF-FSC at 20 °C. Photographs of AF-FSC (a) supporting on soft leaves; (b) bending; (c) twisting. (d) CV and (e) GCD curves of the AF-FSC at different scan rates or current densities. (f) Cycling performance of the AF-FSC at 100 mV s^{-1}.

The good electrochemical performance of AF-FSC could be explained by the pseudocapacitance of PPy on the basis of redox reactions caused by the intercalation of H^+ (eqn (6)):

$$PPy^+ + H^+ + e^- \leftrightarrow PPy^0 \quad (6)$$

An appropriate porous structure and large specific surface area (32.69 m^2 g^{-1}) of the PPy/ADW electrode contributed to promoting electrolyte H^+ transport, leading to a good specific capacitance of AF-FSC.[37,38] Specifically, the ion diffusion in the wood-based electrode is mainly along the cellulose nanofibers and the gaps between the wood cellulose nanofibers, which acted as nanochannels.[39] The high porosity (83%) of PPy/ADW benefited a relatively high loading of electrolyte guests,[40] allowing a rapid electrolyte ion diffusion. Meanwhile, the large pore volume (4.83 cm^3 g^{-1}) also showed good tolerance to the strain relaxation and repeated expansion during the energy storage and release processes.[41]

The device maintained about 90% capacitance after 4000 cycles (Fig. 3f), indicating excellent operational stability for potential application. Nyquist plots measured after 0, 2000 and 4000 cycles at 20 °C (Fig. S10†) were fitted by the equivalent circuit.[41] R_s, R_{ct}, CPE1, and Z_w were the electrolyte resistance, charge transfer resistance at the interface of electrode/electrolyte, double-layer capacitance, and Warburg diffusion resistance, respectively. R_{ct} was 2.007 Ω for AF-FSC at 20 °C and increased to 2.448 and 2.644 Ω after 2000 and 4000 testing cycles, respectively (Table S2†). The small resistance change indicated good conductivity retention of PPy/ADW-based AF-FSC during 4000 testing cycles.[42]

Good environmental adaptability, especially for anti-freezing performance, is critical in the practical application of SC. However, most wood-based SCs only maintain their high electrochemical performance at room temperature; thus, developing anti-freezing wood-based SC is necessary. Since it was reported that decreased temperatures showed nearly no influence on the structure and electrochemical performances of PPy-based SC,[41] the key factor here affecting capacitance was the AF-OHP solid-state electrolyte. Traditional electrolytes, based on water molecules, were frozen to ice at low temperatures, leading to decreasing ionic conductivity and increasing interfacial charge transfer resistance between the electrolyte and electrodes.[31] As a result, such electrolyte-based SCs lost the most electrochemical performance. By introducing EG molecules, AF-OHP maintained a high ionic conductivity under a cold environment, demonstrating an excellent anti-freezing ability. Such high ion conductivity of AF-OHP could be attributed to two main factors.[35] Firstly, EG competes with water molecules to form stable organic molecular clusters, decreasing the saturated vapor pressure of water in the AF-OHP electrolyte. Compared with traditional water-based electrolytes, such as PAM, the lower saturated vapor pressure in AF-OHP contributes to maintaining water molecules at low temperatures and thus enhances the cold tolerance of SC. Secondly, water molecules bridge hydroxyl groups of EG and carbonyl groups of PAM chains, leading to increasing binding energy, so interactions between EG-water mixture and PAM chains are stronger than water–PAM or EG–PAM (Fig. 4a). In this case, water molecules are tightly locked in the AF-OHP network, and the formation of crystal lattices is inhibited. As a result, the prepared AF-FSC is expected to present good electrochemical performance at low temperatures. However, in a cold environment, the increasing electrolyte viscosity could not be prevented completely, leading to decreasing ion transport capability.[34] As a result, the ionic conductivity of the AF-OHP hydrogel electrolyte increased with decreasing temperature (Fig. S11†). AF-OHP had an ionic conductivity of 2.72, 2.17, 2.08, and 1.85 mS cm^{-1} at 20, 0, −15, and −30 °C, respectively. Thus, the specific capacitance of AF-FSC decreased with the drop of temperature, owing to the deceleration of electron/ion transport and electrochemical reactions according to Arrhenius law.[43]

To verify the anti-freezing behavior of AF-FSC, CV and GCD experiments were studied (Fig. 4b, c, S12 and S13†). High areal capacitance of 333.12, 261.45, and 202.05 mF cm^{-2} as well as volume capacitance of 3331.2, 2614.5, and 2020.5 mF cm^{-3} at 6 mA cm^{-2} under 0, −15, and −30 °C were received, respectively,

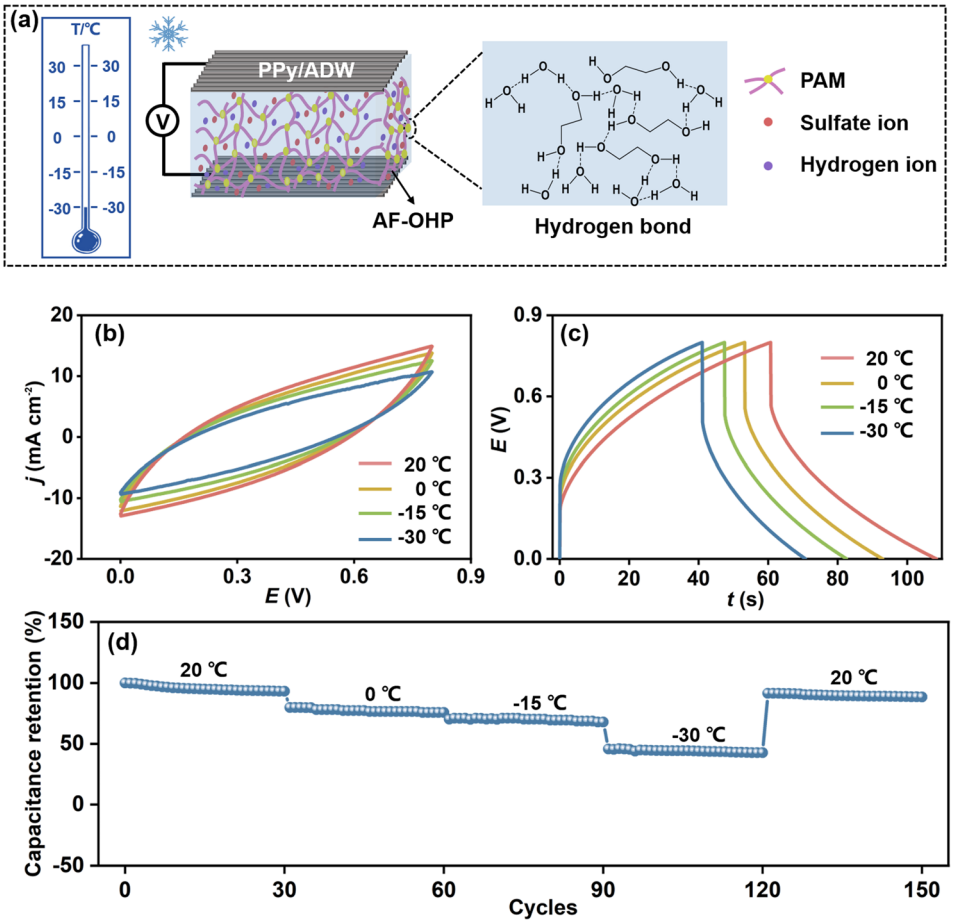

Fig. 4 The anti-freezing property of the SC. (a) Schematic illustration of the SC at −30 °C. Comparison of (b) CV and (c) GCD curves of the SC at temperatures of 20, 0, −15 and −30 °C. (d) Cycling performance of the SC at 20, 0, −15 and −30 °C. Scan rate of CV: 100 mV s^{-1}; current density of GCD: 6 mA cm^{-2}.

which were higher than most wood-based SCs at room temperature.[44–46] Meanwhile, the areal capacitance was stable at the same temperature and completely restored when recovered to 20 °C, proving that AF-FSC could continuously work in a wide temperature range (Fig. 4d).

Furthermore, CV measurements were carried out to examine the stability of AF-FSC in cold environments of −30 °C, and 80% capacitance was maintained after 1000 cycles (Fig. S14†). The outstanding stability of AF-FSC under cold environments could be attributed to the following factors. Firstly, evaporation of water molecules was effectively prevented during long-time testing due to the strong hydrogen bond network between polymer chains and water molecules in AF-OHP. Secondly, there was unnecessary to predefining stretchable structures, thus ensuring stable electrochemical performance of SCs even after a long-term operation. Thirdly, *in situ* growth of PPy both on the surface and inside channels of ADW minimized overall resistance, greatly reducing the distance of ion diffusion at the electrode/electrolyte interface for integrated AF-FSC.

Additionally, the super hydrophilic behavior of PPy/ADW also contributed to distance reduction of ion diffusion at the electrode/electrolyte interface of AF-FSC, enhancing infiltration of the electrolyte. As shown in Fig. 5a, the water droplet completely penetrated PPy/ADW within 1.0 s, while PPy coated natural balsa wood showed a high contact angle of 58° after the same dropping time (Fig. 5b). Moreover, the water droplet was not completely absorbed by PPy coated natural balsa wood after 5 s (Fig. S15a, and b†), indicating good wettability of PPy/ADW. Moreover, electrolyte absorption ability (A) (determined by eqn (5)) of PPy/ADW and PPy coated natural balsa wood was investigated. PPy/ADW demonstrated better absorption capacity with A values up to ≈9.6 (20 °C) and ≈8.2 (−30 °C). Benefiting from the super hydrophilic behavior, electrolyte storage kinetics of PPy/ADW was greatly enhanced, facilitating ion transport at the electrode/electrolyte interface of SC.

Furthermore, AF-FSC also displayed excellent flexibility. Electrochemically, AF-FSC maintained typical CV (Fig. S16a, d and S17a, and d†) and GCD curves (Fig. S16b, e and S17b, and e†). When bending/twisting towards 0–180° at −30 °C, it performed a stable capacitance retention of 97% (Fig. 5d). After repeatedly bent/twisted for 1000 cycles at −30 °C, it retained 93% of initial capacitance (Fig. 5e, S16c, f and S17c, and f†). The outstanding flexibility of AF-FSC could be further explained by two factors. Firstly, the addition of EG effectively prevented the freezing of water molecules and thus maintained the inherent flexibility of AF-FSC. Secondly, strong adhesion between AF-

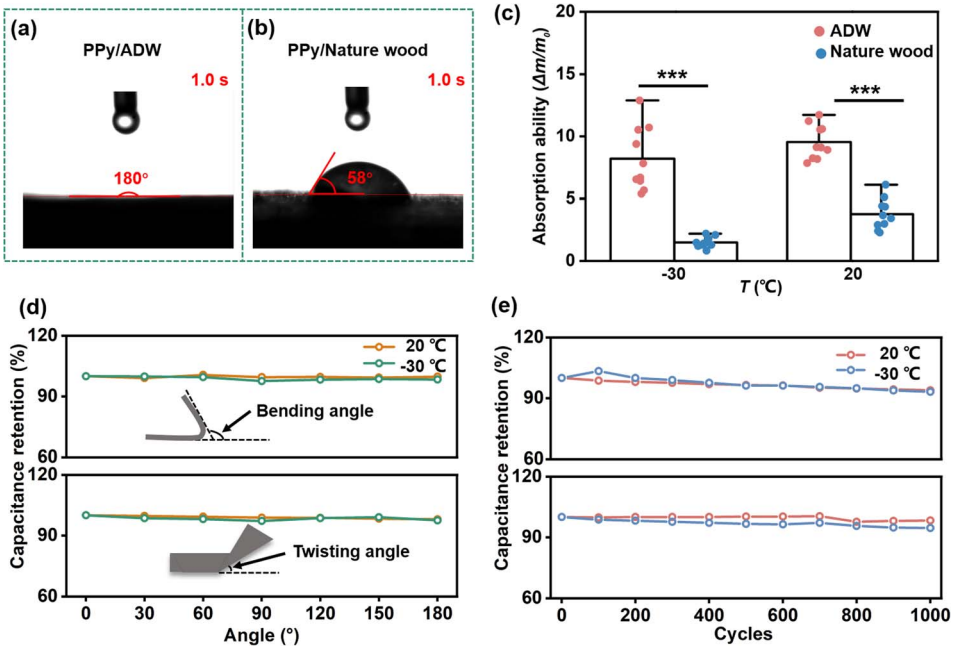

Fig. 5 The intrinsic flexibility of the AF-FSC at 20 or −30 °C. Contact angle of (a) PPy/ADW, (b) PPy/natural balsa wood after dropping a water droplet for 1.0 s at 20 °C. (c) Corresponding electrolyte absorption ability of PPy/ADW (red bar) and natural balsa wood (blue bar) at 20 and −30 °C. Capacitance retention of AF-FSC (d) under different bending/twisting angles; (e) after 1000 bending/twisting cycles.

OHP electrolyte and PPy/ADW electrodes contributed to ensuring the high structural integrity of AF-FSC under the bending/twisting process (Fig. S6†), greatly avoiding delamination between the electrode and electrolyte.

3.3 Application of AF-FSC at ultralow temperature

As a proof of concept, three AF-FSCs with patterns of "D" "U" "T" were connected with a button cell in series in a cold environment (Fig. 6a). Red LEDs, heart-shaped, could be powered by

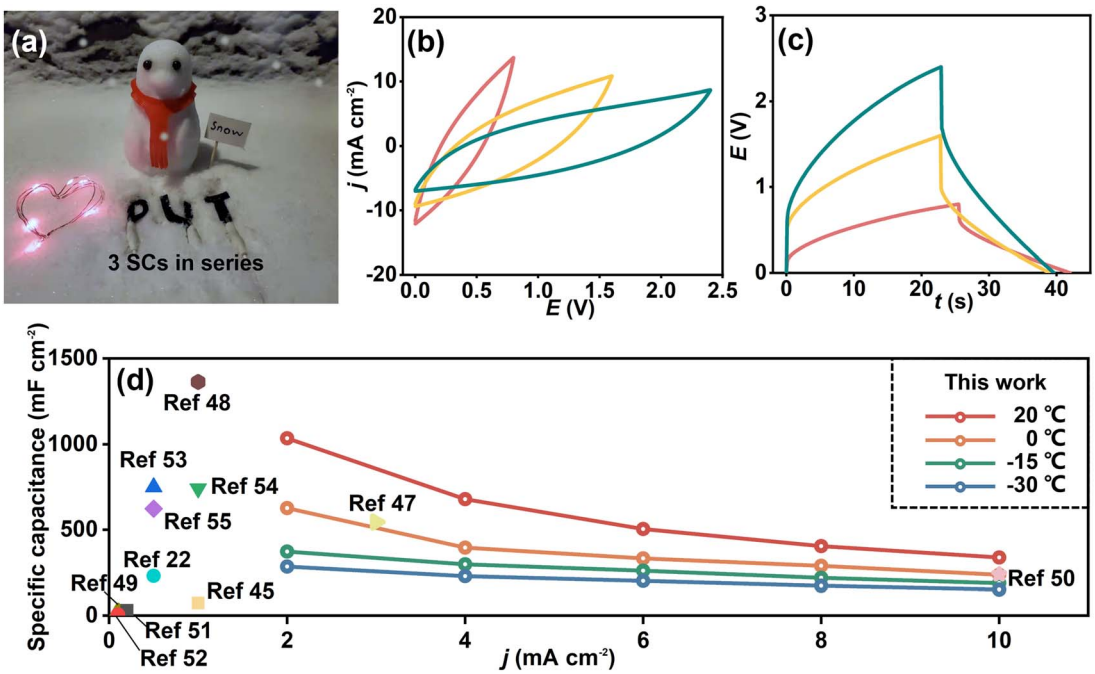

Fig. 6 Demonstrated application of the AF-FSC at ultralow temperature. (a) LED with heart-shape powered by three AF-FSCs and a button cell in series, the patterns of the AF-FSCs with "D", "U", "T" are inspired from the abbreviation of Dalian University of Technology (DUT). (b) CV curves and (c) GCD curves of a single AF-FSC, two AF-FSCs or three AF-FSCs in series. (d) Comparison of specific capacitance with reported wood derivative-based SCs at different temperatures. Scan rate of CV: 100 mV s^{-1}; current density of GCD: 6 mA cm^{-2}.

AF-FSCs, highlighting excellent anti-freezing properties. CV and GCD curves of connected AF-FSCs showed that the output voltage could simply enlarge to 2.4 V by connecting three AF-FSCs in series (Fig. 6b, and c).

Compared with wood derivative-based SCs (Fig. 6d),[22,45,47–55] the as-prepared AF-FSC achieved an outstanding electrochemical performance and anti-freezing properties with high flexibility, which would promote the development of novel wood nanotechnology procedures.

4 Conclusions

In summary, an anti-freezing flexible SC based on soft chemical de-lignified wood-derived electrodes and organohydrogen solid electrolyte was constructed in this work. Taking advantage of the unique structure of the wood electrode, including multi-channels along the tree growth direction and high flexibility, as well as high ionic conductivities of hydrogel electrolyte, the as-prepared AF-FSC demonstrated good flexibility and anti-freezing performance with a specific areal capacitance of 285.2 mF cm^{-2} at 6 mA cm^{-2} under −30 °C. Over 93% capacitance retention was maintained after 1000 bending/twisting cycles at −30 °C, indicating outstanding flexibility of AF-FSC under harsh environments. These performances are far better than those reported for wood-derived SCs. Therefore, the as-obtained wood derivative-based AF-FSC with high flexibility and good stability at low temperatures would promote wood as a potential candidate for fabricating low-cost, green, and portable electronics towards real-life environments.

Data availability

All data generated or analyzed during this study are included in this published article (and its additional files) at **https://doi.org/10.1039/d4ta02190h**. Data will be made available on request.

Author contributions

Nan Zhu conceived the idea and project. Hongting Ma performed the experiment and data analysis. Qian Zhao, Peihao Cheng, Xiaodong Geng, Huannuo Tao, Zhouxiaolong Zhang, Yue Jiang, Junlin Ma, Kai Yang, Quanli Liu, Hanwen Zhang, Zhida Liang, Jian Li, Tianlu Wang and Mianqi Xue performed partial experiment and data analysis. Nan Zhu and Hongting Ma discussed the results and wrote the paper.

Conflicts of interest

There are no conflicts to declare.

Acknowledgements

We are grateful for the financial support from the National Natural Science Foundation of China (Grant No. 22211530046; 22074010), the Fundamental Research Funds for the Central Universities (Grant No. DUT23YG128), State Key Laboratory of New Textile Materials and Advanced Processing Technologies (Grant No. FZ2023009). The authors acknowledge the assistance of the Instrumental Analysis Center, Dalian University of Technology, China.

Notes and references

1 Poonam, K. Sharma, A. Arora and S. K. Tripathi, *J. Energy Storage*, 2019, **21**, 801–825.
2 S. Kumar, G. Saeed, L. Zhu, K. N. Hui, N. H. Kim and J. H. Lee, *Chem. Eng. J.*, 2021, **43**, 126532.
3 R. Bird, Z. J. Baum, X. Yu and J. Ma, *ACS Energy Lett.*, 2022, **7**, 736–740.
4 D. Hubble, D. E. Brown, Y. Zhao, C. Fang, J. Lau, B. D. McCloskey and G. Liu, *Energy Environ. Sci.*, 2022, **15**, 550–578.
5 T. Liu, J. P. Vivek, E. W. Zhao, J. Lei, N. Garcia-Araez and C. P. Grey, *Chem. Rev.*, 2020, **120**, 6558–6625.
6 F. Duffner, N. Kronemeyer, J. Tübke, J. Leker, M. Winter and R. Schmuch, *Nat. Energy*, 2021, **6**, 123–134.
7 G. Zhang, J. Hu, Y. Nie, Y. Zhao, L. Wang, Y. Li, H. Liu, L. Tang, X. Zhang, D. Li, L. Sun and H. Duan, *Adv. Funct. Mater.*, 2021, **31**, 2100290.
8 D. P. Chatterjee and A. K. Nandi, *J. Mater. Chem. A*, 2021, **9**, 15880–15918.
9 P. Lamba, P. Singh, P. Singh, P. Singh, Bharti, A. Kumar, M. Gupta and Y. Kumar, *J. Energy Storage*, 2022, **48**, 103871.
10 S. Dai, Y. Bai, W. Shen, S. Zhang, H. Hu, J. Fu, X. Wang, C. Hu and M. Liu, *J. Power Sources*, 2021, **482**, 228915.
11 T. Wang, K. Li, Q. Le, S. Zhu, X. Guo, D. Jiang and Y. Zhang, *J. Colloid Interface Sci.*, 2021, **594**, 812–823.
12 G. Manibalan, Y. Govindaraj, J. Yesuraj, P. Kuppusami, G. Murugadoss, R. Murugavel and M. Rajesh Kumar, *J. Colloid Interface Sci.*, 2021, **585**, 505–518.
13 H. Liu, J. Zhu, Z. Li, Z. Shi, J. Zhu and H. Mei, *Chem. Eng. J.*, 2021, **403**, 126325.
14 J. Chen, L. Wei, A. Mahmood, Z. Pei, Z. Zhou, X. Chen and Y. Chen, *Energy Storage Mater.*, 2020, **25**, 585–612.
15 W. Jiang, T. Wang, H. Chen, X. Suo, J. Liang, W. Zhu, H. Li and S. Dai, *Nano Energy*, 2021, **79**, 105464.
16 M. B. Arvas, H. Gürsu, M. Gencten and Y. Sahin, *J. Energy Storage*, 2021, **35**, 102328.
17 T. Xu, D. Yang, S. Zhang, T. Zhao, M. Zhang and Z.-Z. Yu, *Carbon*, 2021, **171**, 201–210.
18 C. Chen, Y. Wang, Q. Wu, Z. Wan, D. Li and Y. Jin, *Chem. Eng. J.*, 2020, **400**, 125876.
19 Z. Qiu, Z. Xiao, L. Gao, J. Li, H. Wang, Y. Wang and Y. Xie, *Compos. Sci. Technol.*, 2019, **172**, 43–48.
20 G. Yan, S. He, G. Chen, S. Ma, A. Zeng, B. Chen, S. Yang, X. Tang, Y. Sun, F. Xu, L. Lin and X. Zeng, *Nano-Micro Lett.*, 2022, **14**, 84.
21 C. Chen, Y. Zhang, Y. Li, J. Dai, J. Song, Y. Yao, Y. Gong, I. Kierzewski, J. Xie and L. Hu, *Energy Environ. Sci.*, 2017, **10**, 538–545.
22 Y. Zhao, Y. Alsaid, B. Yao, Y. Zhang, B. Zhang, N. Bhuskute, S. Wu and X. He, *Adv. Funct. Mater.*, 2020, **30**, 1909133.
23 W. Zhang, Y. Yang, R. Xia, Y. Li, J. Zhao, L. Lin, J. Cao, Q. Wang, Y. Liu and H. Guo, *Carbon*, 2020, **162**, 114–123.

24 W. Leng, S. Zhai and B. Pan, *Cellulose*, 2019, **26**, 8685–8697.
25 Z. Li, C. Chen, H. Xie, Y. Yao, X. Zhang, A. Brozena, J. Li, Y. Ding, X. Zhao, M. Hong, H. Qiao, L. M. Smith, X. Pan, R. Briber, S. Q. Shi and L. Hu, *Nat Sustainability*, 2021, **5**, 235–244.
26 H. Bian, J. Luo, R. Wang, X. Zhou, S. Ni, R. Shi, G. Fang and H. Dai, *ACS Sustain. Chem. Eng.*, 2019, **7**, 20022–20031.
27 Y. Song, W. Chen, X. Niu, G. Fang, H. Min and H. Pan, *ChemSusChem*, 2018, **11**, 3714–3718.
28 J. Song, C. Chen, C. Wang, Y. Kuang, Y. Li, F. Jiang, Y. Li, E. Hitz, Y. Zhang, B. Liu, A. Gong, H. Bian, J. Y. Zhu, J. Zhang, J. Li and L. Hu, *ACS Appl. Mater. Interfaces*, 2017, **9**, 23520–23527.
29 X. Jin, L. Song, H. Yang, C. Dai, Y. Xiao, X. Zhang, Y. Han, C. Bai, B. Lu, Q. Liu, Y. Zhao, J. Zhang, Z. Zhang and L. Qu, *Energy Environ. Sci.*, 2021, **14**, 3075–3085.
30 L. Lan, L. Li, Q. Di, X. Yang, X. Liu, P. Naumov and H. Zhang, *Adv. Mater.*, 2022, **34**, e2200471.
31 S. Jayaraman, T. J. Rawson and M. A. Belyustina, *Energy Environ. Sci.*, 2022, **15**, 2948.
32 K. Abe and H. Yano, *Carbohydr. Polym.*, 2011, **85**, 733–737.
33 H. Ma, F. Lv, L. Shen, K. Yang, Y. Jiang, J. Ma, X. Geng, T. Sun, Y. Pan, Z. Xie, M. Xue and N. Zhu, *Energy Environ. Mater.*, 2022, **5**, 986–995.
34 Z. Liu, J. Zhang, J. Liu, Y. Long, L. Fang, Q. Wang and T. Liu, *J. Mater. Chem. A*, 2020, **8**, 6219–6228.
35 F. Mo, G. Liang, Q. Meng, Z. Liu, H. Li, J. Fan and C. Zhi, *Energy Environ. Sci.*, 2019, **12**, 706–715.
36 T. Chen, R. Hao, H. Peng and L. Dai, *Angew Chem. Int. Ed. Engl.*, 2015, **54**, 618–622.
37 X. Hu, L. Fan, G. Qin, Z. Shen, J. Chen, M. Wang, J. Yang and Q. Chen, *J. Power Sources*, 2019, **414**, 201–209.
38 J. Liu and P. Liu, *J. Colloid Interface Sci.*, 2019, **542**, 1–7.
39 G. Chen, T. Li, C. Chen, W. Kong, M. Jiao, B. Jiang, Q. Xia, Z. Liang, Y. Liu, S. He and L. Hu, *ACS Nano*, 2021, **15**(7), 11244–11252.
40 C. Young, J. Lin, J. Wang, B. Ding, X. Zhang, S. M. Alshehri, T. Ahamad, R. R. Salunkhe, S. A. Hossain, J. H. Khan, Y. Ide, J. Kim, J. Henzie and K. C. W. Wu, *Chem.–Eur. J.*, 2018, **24**(23), 6127–6132.
41 Q. Zhang, Y. Li, J. Zhu, L. Lan, C. Li, J. Mao, F. Wang, Z. Zhang and L. Wang, *Chem. Eng. J.*, 2021, **420**, 129712.
42 L. Pan, G. Yu, D. Zhai, H. R. Lee, W. Zhao, N. Liu, H. Wang, B. C. K. Tee, Y. Shi, Y. Cui and Z. Bao, *Proc. Natl. Acad. Sci. U. S. A.*, 2012, **109**, 9287–9292.
43 X. Zang, R. Zhang, Z. Zhen, W. Lai, C. Yang, F. Kang and H. Zhu, *Nano Energy*, 2017, **40**, 224–232.
44 C. Chen and L. Hu, *Acc. Chem. Res.*, 2018, **51**, 3154–3165.
45 J. Cao, Y. Zhao, Y. Xu, Y. Zhang, B. Zhang and H. Peng, *J. Mater. Chem. A*, 2018, **6**, 3355–3360.
46 M. Wang, L. Fan, G. Qin, X. Hu, Y. Wang, C. Wang, J. Yang and Q. Chen, *J. Membr. Sci.*, 2020, **597**, 117740.
47 H. Xu, X. Hu, H. Yang, Y. Sun, C. Hu and Y. Huang, *Adv. Energy Mater.*, 2015, **5**, 1401882.
48 K. Liu, R. Mo, W. Dong, W. Zhao and F. Huang, *J. Mater. Chem. A*, 2020, **8**, 20072–20081.
49 L. Liu, Z. Ji, S. Zhao, Q. Niu and S. Hu, *J. Mater. Chem. A*, 2021, **9**, 6172–6179.
50 W. Wu, X. Wang, Y. Deng, C. Zhou, Z. Wang, M. Zhang, X. Li, Y. Wu, Y. Luo and D. Chen, *Nanoscale*, 2020, **12**, 17738–17745.
51 Y.-R. Kim, H. K. Nam, Y. Lee, D. Yang, T.-S. D. Le, S.-W. Kim, S. Park and Y.-J. Kim, *Biochar*, 2024, **6**, 36.
52 S. L. Silvestre, T. Pinheiro, A. C. Marques, J. Deuermeier, J. Coelho, R. Martins, L. Pereira and E. Fortunato, *Flexible Printed Electron.*, 2022, **7**(3), 035021.
53 D. Zhang, K. Yang, T. Zhang, M. Luo, M. Li, Z. Li, C. Liu, Y. Ling, W. Chen and X. Zhou, *Chem. Eng. J.*, 2023, **460**, 141733.
54 W. Zhang, Y. Pang, B. Wang, H. Guo and Y. Liu, *Diamond Relat. Mater.*, 2024, **141**, 110684.
55 M. Luo, D. Zhang, K. Yang, Z. Li, Y. Hu, S. Xia, W. Chen and X. Zhou, *Fuel Process. Technol.*, 2022, **238**, 107496.

